Journal of Membrane Science 394–395 (2012) 175–183

Contents lists available at SciVerse ScienceDirect

Journal of Membrane Science

journal homepage: www.elsevier.com/locate/memsci

Relationship between morphology and conductivity of block-copolymer based battery separators

David T. Wong[a,b], Scott A. Mullin[a,b], Vincent S. Battaglia[b], Nitash P. Balsara[a,b,*]

[a] Department of Chemical and Biomolecular Engineering, University of California, Berkeley, CA 94720, USA
[b] Environmental Energy Technologies Division, Lawrence Berkeley National Laboratory, Berkeley, CA 94720, USA

ARTICLE INFO

Article history:
Received 18 July 2011
Received in revised form 7 December 2011
Accepted 23 December 2011
Available online 31 December 2011

Keywords:
Battery separator
Nanoporous
Block copolymer blends
Morphology effect
Ionic conductivity

ABSTRACT

Nanoporous battery separators were made by blending a polystyrene-*block*-polyethylene-*block*-polystyrene copolymer (SES) and polystyrene (PS) homopolymers, casting films of the blend, and selectively dissolving the homopolymer. The efficacy of the separators thus obtained was determined by measurement of the ionic conductivity of separators soaked in 1 M lithium hexafluorophosphate in ethylene carbonate/diethyl carbonate (1:1, v/v, Novolyte Technologies, Inc.), a standard lithium battery electrolyte. We focus on the effect of chain length of the sacrificial homopolymer on separator morphology and ion transport. In highly porous separators with a nominal pore volume fraction of 0.43, conductivity peaked at $\alpha = 0.22$, where values as high as 0.39 mS cm^{-1} were achieved (α is the molecular weight of the PS homopolymer normalized by that of the PS block in the SES copolymer). Nitrogen adsorption experiments and scanning electron microscopy were used to determine the underpinnings of this observation. At $\alpha = 0.12$, extremely small pores with low surface area are formed. Increasing α to 0.22 results in a film with well-connected nanoscale pores. A further increase in α to 2.02 results in films with micron-sized pores that are not effective for ion transport.

1. Introduction

Nanoporous separators used in lithium ion technology are presently of considerable interest in spite of the fact that they are an inactive component of the battery. In most cases, the separators are composed of inert semi-crystalline polyolefins such as polyethylene or polypropylene. A liquid electrolyte contained in the pores is responsible for ion transport in the battery. Although these polyolefin materials only cost about 1.30 $ per kg, the cost of a typical battery separator is in the vicinity of 120–240 $ per kg [1]. This large increase in price is mainly due to the complex and carefully controlled processing steps used to generate the porous structure within the separator.

There are two different approaches for generating pores in battery separators: wet processes and dry processes. In wet processes, a membrane comprising a phase-separated mixture of an amorphous and a semi-crystalline polyolefin is immersed in a solvent at room temperature. Semi-crystalline polyolefins are typically soluble at elevated temperatures in the vicinity of the melting temperature. During solvent treatment only the amorphous polyolefin is solvated and removed, thus leaving behind a porous semi-crystalline structure [2–4]. In addition, films made by wet processes are stretched either before or after extraction to increase porosity, resulting in slightly oriented pore structures. In dry processes, pores are produced entirely by stretching semi-crystalline polyolefin films. Pores are generated because the deformation tends to be localized in the amorphous regions of the semi-crystalline polyolefins. The pores obtained by dry processes tend to be straight and oriented perpendicular to the plane of the film. Uniaxially oriented films produced from dry methods have high tensile strengths only in the stretching direction, while films produced using the wet method typically have high tensile strength in all directions. The balance of tensile strength is not necessarily advantageous as tensile strength is primarily important for roll-to-roll battery manufacturing wherein films are pulled along one axis only [2]. Separators made via dry processes exhibit significantly lower tortuosities than those made via wet processes. Typically, separators made by dry processes are better suited for high power density applications, while those made by wet processes are better suited for long battery life applications. This is because the straight pores in separators made from the dry process allow a more direct path for ions to travel (higher power density), while separators made through the wet process are more tortuous and can suppress dendritic lithium that may form on the graphite anode (longer life)

* Corresponding author at: Department of Chemical and Biomolecular Engineering, University of California, Berkeley, CA 94720, USA. Tel.: +1 510 642 8973; fax: +1 510 642 4778.
E-mail address: nbalsara@berkeley.edu (N.P. Balsara).

0376-7388/$ – see front matter © 2012 Elsevier B.V. All rights reserved.
doi:10.1016/j.memsci.2011.12.037

[4]. The uniformity of the resulting pore structures is crucial for battery performance. Non-uniform pore structures will lead to non-uniform current distributions during battery operation. Defects in the separator can lead to catastrophic failure of batteries.

In conventional wet processes, the extent of phase separation in the membrane prior to the pore formation step is determined entirely by non-equilibrium effects [5–9]. This is because phase-separated structures that are created by blending immiscible substances above their melting temperatures (e.g. oil and water) will continue to coarsen until the heavier phase settles to the bottom of the container. In the case of polymers, this process is extremely slow due to slow molecular motion [10–12] and it is thus feasible to trap phase-separated structures with characteristic length scales ranging from nanometers to microns. However, small changes in the processing conditions can lead to large changes in the phase-separated morphology which, in turn, affects pore structure. Since driving forces for phase-separation in polymers depend crucially on the molecular weight of the components [13,14], small changes in the molecular weight distributions of the amorphous and semi-crystalline components can also result in alterations of the pore structure [15–18]. This is a significant problem because commercial approaches for synthesizing polyolefins often lead to very broad molecular weight distributions. In this paper we describe a new wet process that utilizes blends of anionically synthesized model block copolymers and homopolymers with relatively narrow molecular weight distributions to address these problems.

The membranes studied in this paper are composed of a polystyrene-*block*-polyethylene-*block*-polystyrene (SES) copolymer. The driving forces that lead to the formation of periodic microphase-separated structures in block copolymers are well-established [19–21]. The immiscibility of polystyrene (PS) and polyethylene (PE) results in phase-separation, but the covalent bond between the PS and PE chains restricts the size of the phase-separated domains to molecular dimensions (typically 10–50 nm). The size of the domains is governed by chain length, whereas the geometry of the microphases (e.g. lamellar or cylindrical) is governed by the PS-to-PE ratio. Depending on the balance between thermodynamic and kinetic driving forces, the PE crystals can either be trapped within the microphases or break out of them, as quantified by Register, Ryan and coworkers [22–29]. In the first step of our process, a non-porous membrane is made by solvent-casting a mixture of SES and PS. In the simplest case, the PS homopolymer simply swells the PS microphase of the block copolymer. Selective dissolution of PS (which is amorphous) results in the formation of nanoscale pores in a polyethylene matrix. There are two crucial differences between the present process and those formed in conventional wet processes. First, the phase-separated morphology that is the basis for the porous structure of the final membrane is at equilibrium and thus strict control of processing conditions during the first film forming step is not essential. Second, the pores are naturally lined with PS chains because of the structure of the SES copolymer. Since PS is slightly more polar than PE, it may lead to more complete filling of the porous structure with the electrolyte, which is especially of concern for structures with small-diameter pores [30,31]. Although the functioning separators in this work are comprised entirely of the SES copolymer, this paper focuses on the role of the sacrificial PS homopolymers. In particular, we show that choosing the correct molecular weight of the sacrificial PS homopolymer to blend with the SES copolymer is crucial for obtaining membranes with well-connected pore structures.

While the present study is primarily motivated by fundamental aspects of the relationship between morphology and ion transport, the membranes described herein may also be of practical interest. Material costs of PE-containing block copolymers are about an order of magnitude higher than those of PE homopolymers. However, the simplicity of the proposed processing steps has the potential to reduce the overall cost of the finished separators.

The proposed approach of creating nanoporous block copolymer films has been used by others for a wide range of applications ranging from water filtration to drug delivery [32–36]. Phillip et al. generated monolithic nanoporous materials by synthesizing poly(DL-lactide)-*block*-polydimethylsiloxane-*block*-polystyrene, shear aligning the polymer, and selectively etching out the lactide block [32]. They generated membranes with well-defined cylindrical pores with diameters of about 15 nm and found that gas flow through the membranes followed Knudsen diffusion, while liquid flow obeyed the well-established Hagen–Poiseuille equation. Uehara et al. created porous films by exposing polystyrene-*block*-polyethylene copolymer films to fuming nitric acid [33]. Nitric acid selectively etches the PS microphase, which enables control of the pore diameter by adjusting exposure time. This enabled a systematic study of the effect of pore size on the diffusion of glucose and albumin. Yang et al. obtained films by spin-coating blends of homopolymer poly(methyl methacrylate) (PMMA) and polystyrene-*block*-poly(methyl methacrylate) [34,35]. The PMMA homopolymer was selectively dissolved, leaving behind cylindrical pores with a diameter of 15 nm. The diameter of the holes was reduced by deposition of gold inside the holes. This enabled a systematic study of the effect of pore size on drug release. Zhou et al. made films comprising polyisoprene (PI), PS, and a polyisoprene-*block*-polystyrene copolymer [36]. The concentrations of the components were chosen so that a bicontinuous microemulsion morphology was obtained. Crosslinking the PI chains enabled selective dissolution of the PS homopolymer, leaving pores with average diameters of approximately 45 nm. By comparing the conductivity of the membrane swollen with an ionic liquid with that of the pure ionic liquid, Zhou et al. concluded that their membrane had a tortuosity factor of about 2.

2. Experimental

2.1. Synthesis and characterization of polymers

A polystyrene-*block*-polybutadiene (SB) copolymer was synthesized by anionic polymerization using *sec*-butyl lithium as the initiator [37]. The living chains were coupled using dibromoethane to produce a symmetric SBS triblock copolymer [38]. The use of a nonpolar solvent (cyclohexane) results in polybutadiene chains with approximately 93% 1,4-addition. SBS was saturated using *p*-toluenesulfonyl hydrazide in the presence of equimolar tri-*n*-propyl amine [39]. Homopolymer PS was also synthesized by anionic polymerization using *sec*-butyl lithium as the initiator. The molecular weights of the PS and PE blocks for the SES copolymer were 15 and 82 kg mol^{-1}, respectively, and the PE volume fraction, $\phi_{PE,BCP}$, was 0.77 (in the melt state at 140 °C). The melt densities used for PE, PS, and SES are 0.78, 0.97, and 0.83 g cm^{-3}, respectively, at 140 °C [40]. Six different PS homopolymers were synthesized with molecular weights ranging from 1.8 kg mol^{-1} to 30 kg mol^{-1}. The molecular weight of the PS block of the SBS copolymer was obtained by extracting an aliquot of the reaction mixture during synthesis prior to butadiene addition. The PS molecular weight was measured on a Viscotek GPC Max VE-2001 equipped with a TDA 302 triple-detector system calibrated using PS standards with tetrahydrofuran (THF) as the eluent. The volume fractions of each block of the SBS copolymer and the ratio of 1–2 versus 1–4 vinyl addition in the polybutadiene (PB) blocks of the copolymer were determined using ^{1}H nuclear magnetic resonance (NMR) spectroscopy ($CDCl_3$, 25 °C). High temperature NMR (toluene–d_8, 90 °C) was used to ensure the complete saturation of the vinyl groups in the

polybutadiene block of the SES copolymer. The polydispersity indices of the homopolymers were less than 1.06. The coupling reaction used to synthesize the triblock was not perfect resulting in 76% triblock and 24% diblock. The polydispersity indices of the two populations of chains were about 1.02.

To remove saturation reagents, SES copolymers were precipitated in methanol, redissolved in *o*-xylene at 100 °C, and then washed in a separatory funnel with excess deionized water. This procedure was repeated three times. The polymer was then dried under vacuum at 80 °C for 2 days. PS homopolymers were purified by precipitation in methanol. The homopolymers were then redissolved in benzene and precipitated two more times, filtered through a 0.2 μm filter, and freeze-dried in a lyophilizer (Millrock LD85).

2.2. Film preparation

Films of SES/PS blends were prepared using a custom-built solvent caster consisting of a doctor blade to control film thickness and a heated stage to control film temperature. The caster was located in an argon glovebox with a solvent trap. The top surface of the solvent caster consists of a porous aluminum vacuum plate, upon which fresh sheets of aluminum foil are applied to create pristine substrates. Solutions of SES, PS, and *o*-xylene were prepared at 120 °C and doctor-bladed onto aluminum foil at 80 °C. The smoothness and thickness of the films depended mainly on the SES concentration, and 0.05 g SES per mL *o*-xylene was used to create the films in this study. After drying the film on the caster for 15 min at 80 °C, the films were further dried at 80 °C in a vacuum oven for 12 h. The aluminum foil was separated from the polymer film by immersion in 1 M hydrochloric acid. Resultant free-standing films were dried in a vacuum oven for 4 h, and washed in excess tetrahydrofuran (THF) at room temperature. This resulted in the complete removal of the PS homopolymer. Films were washed in methanol before a final drying step (25 °C in a vacuum oven for 4 h) to produce the porous separators. In all cases, the difference in mass of the films, measured before and after the THF-washing and subsequent drying steps, was within experimental error of the mass of homopolymer PS added in the first step (±2%). We thus define the nominal void fraction, ϕ_V, as the fraction of volume occupied by the PS homopolymer in the SES/PS mixture prior to dissolution. ϕ_V is calculated from the composition of the films and densities of PE, PS, and SES at 140 °C (same densities as in Section 2.1). Our estimate of ϕ_V does not account for changes in volume due to crystallization of PE, vitrification of PS, or changes in the pore geometry that may arise during cooling. We define α as the ratio of the molecular weight of the PS homopolymer to that of the PS in the block copolymer (the latter is 15 kg mol^{-1}). For the blends at any given ϕ_V, the same mass of PS homopolymer is added regardless of α. The nanoporous films used in this study are characterized by two parameters: ϕ_V and α.

The properties of the films thus produced are compared with a commercially available Celgard® 2400 membrane, a polypropylene battery separator made using the dry process. We assume that $\phi_V = 0.37$ for the Celgard® 2400 membrane, as specified by the manufacturer in 2005.

2.3. Ionic conductivity measurements

Conductivity measurements were performed using Swagelok cells with polished electrodes having a diameter of 22.2 mm. Polymer samples were cut out using a 22.2 mm diameter punch, weighed, and then placed into a standard lithium battery electrolyte solution of 1 M lithium hexafluorophosphate ($LiPF_6$) in ethylene carbonate/diethyl carbonate (1:1, v/v, Novolyte Technologies, Inc.) for at least 2 days. The swollen films were placed in the Swagelok cells and the impedance was measured using a potentiostat (Bio-Logic VMP3) over a frequency range from 1 MHz to 500 mHz at a peak-to-peak amplitude voltage of 10 mV. Conductivity, σ, was calculated using the equation $\sigma = l/AR_b$, where A is the electrode area, l is the measured sample thickness, and R_b is the bulk resistance determined from the intersection of the impedance data with the real axis on the Nyquist plot. For samples with higher resistance, the sample resistance was taken as the low frequency minimum of semi-circles obtained in the Nyquist plot. All conductivity measurements were taken at room temperature. The thickness of the samples l, used in the conductivity calculations was measured using a micrometer after the impedance spectroscopy measurements were completed. This thickness was about 10% less than that of the dry electrolyte films due to effects such as plastic deformation under the applied stress in the conductivity cell. Electrolyte uptake measurements were made by blotting electrolyte-swollen films and weighing them after conductivity and film thickness measurements. The volume fraction of electrolyte in the film, ϕ_E, was calculated from the known weights of the dry film and the electrolyte uptake, using the room temperature densities of the polymer [41] and the electrolyte ($\rho_{elec} = 1.26\,g\,cm^{-3}$, $\rho_{poly} = 0.96\,g\,cm^{-3}$ for the block copolymer, and $\rho_{poly} = 0.78\,g\,cm^{-3}$ for Celgard® 2400), ignoring the possibility of non-ideal mixing between SES and the electrolyte. ϕ_E is $\left[(m_{swollen} - m_{dry})(1 - \phi_V)\right] / \left[\rho_{elec}(m_{dry}/\rho_{poly})\right]$, where m_{dry} and $m_{swollen}$ are the dry and swollen weights of the film.

2.4. Nitrogen physisorption experiments

Nitrogen physisorption experiments were performed using a Micromeritics TriStar II instrument. Polymer films were cut into strips and dried under vacuum for 4 h prior to the measurements. The Brunauer–Emmett–Teller (BET) method was employed to calculate an internal surface area for the films [42]. The specific surface area, a_s(BET) can be calculated using:

$$a_s(\mathrm{BET}) = \frac{n_m^a L a_m}{m} \tag{1}$$

where L is Avogadro's number, a_m is the area per molecule of a monolayer, which is 0.162 nm^2 for N_2, m is the mass of the absorbent, and n_m^a is the monolayer capacity. The monolayer capacity was calculated by fitting data to the linear BET equation,

$$\frac{p}{n^a(p^o - p)} = \frac{1}{n_m^a C} + \frac{C-1}{n_m^a C}\frac{p}{p^o} \tag{2}$$

where p is the equilibrium pressure, p^o is the saturation pressure, C is a fitting parameter related to the enthalpy of adsorption, and n^a is the measured volume of nitrogen adsorbed. Parameters C and n_m^a were obtained by fitting the data obtained at low p/p^o values. Further interpretation of physisorption data was based on IUPAC recommendations [43].

2.5. Scanning electron microscopy

Scanning electron microscopy (SEM) images were taken using a Hitachi S-5000 Scanning Electron Microscope. Cast films were cryofractured in liquid nitrogen, loaded onto a brass stub using carbon tape, and sputter coated with Au/Pd before imaging.

2.6. Small angle X-ray scattering

Small angle X-ray scattering (SAXS) experiments were used to characterize the morphology of the battery separators. Measurements were performed at beamline 7.3.3 at the Advanced Light Source at Lawrence Berkeley National Laboratories. Separator films were studied as cast, before and after washing with THF and methanol. Samples were stacked to a thickness of approximately

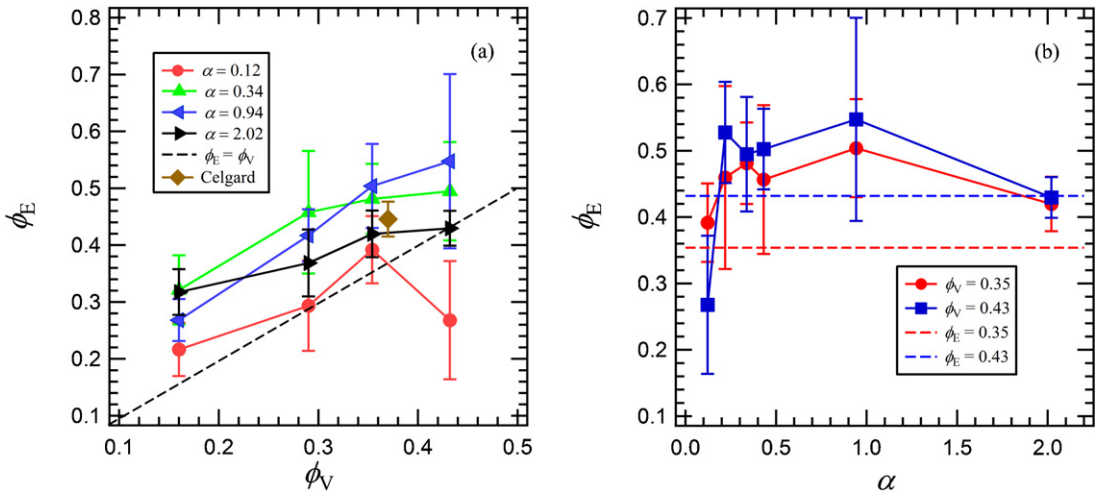

Fig. 1. Electrolyte volume fraction in the separator, ϕ_E, as a function of (a) void fraction, ϕ_V, for select values of the normalized chain length of the sacrificial homopolymer, α and (b) α at $\phi_V = 0.35$ and 0.43. The dashed line in (a) represents $\phi_E = \phi_V$. The dashed lines in (b) represent $\phi_E = \phi_V = 0.35$ and $\phi_E = \phi_V = 0.43$.

100 μm to increase scattering volume and placed between Kapton films. A silver behenate sample was used as a standard, and data were reduced using the Nika program for Igor Pro available from Jan Ilavsky at the Advanced Photon Source. The azimuthally averaged scattering intensity, I, is reported as a function of the scattering vector q ($q = 4\pi \sin(\theta/2)/\lambda$), where θ is the scattering angle and λ is the wavelength of the incident beam).

2.7. Error analysis

Most of the properties reported here are mean values based on measurements on four or five independent samples. The reported error bars represent the standard deviation of the measurements. We do not report error estimates in the BET analysis because only one experiment was run (sample quantity limitations).

3. Results and discussion

3.1. Structure and morphology characterization

In Fig. 1a we plot the electrolyte volume fraction, ϕ_E, versus void volume fraction, ϕ_V, for films with selected values of α. Also included in Fig. 1a is our data obtained from Celgard® 2400. The dashed line in Fig. 1a, a line through the origin with slope = 1, represents the expectation that $\phi_E = \phi_V$. It is evident that in most cases, $\phi_E \approx \phi_V$ (within experimental error). This implies that the nominal pore volume generated by our process is filled with electrolyte, regardless of void fraction and homopolymer chain length. The electrolyte uptake of our separators is similar to that of Celgard® 2400 when void fraction is matched. Regardless of α, ϕ_E increases with increasing ϕ_V. The only significant exception is at $\alpha = 0.12$ and $\phi_V = 0.43$, where ϕ_E is significantly lower than expected. In most cases, the data in Fig. 1a lie slightly above the $\phi_E \approx \phi_V$ line. This is probably due to the elasticity of the separator. We plot ϕ_E as a function of α in Fig. 1b at fixed ϕ_V of 0.35 and 0.43. We focus on this range of ϕ_V because current commercial separators have void volume fractions in this range. The lines in Fig. 1b represent the expected value of ϕ_E for ϕ_V values of 0.35 and 0.43. It is clear that ϕ_E is a weak function of α when α exceeds 0.12. In other words, the amount of electrolyte in our films is not affected by the molecular weight of the sacrificial homopolymer above $\alpha = 0.12$.

In Fig. 2 we show typical results of nitrogen physisorption experiments, where the volume of nitrogen absorbed in the separator, n^a, is plotted as a function of relative pressure, p/p^o, during nitrogen adsorption and desorption. We show data for selected values of α at $\phi_V = 0.43$. The peak seen at high p/p^o in Fig. 2 is expected in the case of slit-like pores. The hysteresis in adsorption and desorption indicates the presence of nanoscale pores. As α increases from 0.22 (Fig. 2a) to 0.34 (Fig. 2b), we see a significant increase in the amount of N_2 adsorbed, which indicates an increase in nanoporosity. Further increasing α to 0.94 results in a decrease in the amount of N_2 adsorbed. Finally, at $\alpha = 2.02$, we see very low amounts of nitrogen adsorption (Fig. 2d), which suggests the presence of very few nanopores in the membranes. The data in Fig. 2 indicate that the internal pore structure in our membranes at fixed ϕ_V is a sensitive function of α (similar data were obtained at other values of ϕ_V).

In Fig. 3, the internal surface area, a_s(BET), calculated using Eqs. (1) and (2), is plotted versus α for films with $\phi_V = 0.35$ and 0.43 (same sample set is shown in Fig. 1b). We find that a_s(BET) is peaked in the vicinity of $\alpha = 0.43$ for both void fractions. These data indicate that separators with intermediate values of α have more accessible pores than those made with either very small values of α (e.g. 0.12) or very large values of α (e.g. 2.02).

Typical position-space images of the pore structure in our films, obtained by SEM, are presented in Fig. 4, where micrographs obtained at $\phi_V = 0.43$ are shown. The cross-sectional view in Fig. 4a shows that $\alpha = 0.12$ results in a very fine porous structure. Larger nanoscale pores can be seen in the film cross-sections at intermediate α values of 0.22 and 0.43 (Fig. 4b and c). Fig. 4d shows an interesting morphology of well-defined pores at $\alpha = 2.03$, but the pore diameters are in the micron range. The SEM data thus confirms our earlier conclusion regarding the reduction in internal surface area in the $\alpha = 2.02$, $\phi_V = 0.43$ membrane.

3.2. Ionic conductivity

In Fig. 5a we plot ionic conductivity, σ, versus α for the $\phi_V = 0.43$ membranes. Membrane conductivity peaks at $\alpha = 0.22$ with a value of 0.39 mS cm^{-1}, which is comparable to that of Celgard® 2400. The conductivity peak in Fig. 5a is highly asymmetric. It decreases precipitously when α decreases from 0.22 to 0.12. In contrast, the conductivity decreases gradually as α is increased from 0.22 to 2.02. Quite surprisingly, the ionic conductivity at $\alpha = 0.12$ and 2.02 are similar. Another feature worth noting is that the size of the error bars for the $\phi_V = 0.43$ membranes are relatively small. In Fig. 5b, we plot σ versus α for the values of ϕ_V less than 0.43. At $\phi_V = 0.16$, $\sigma = 0.03$ mS cm^{-1} regardless of the value of α. This value is considerably smaller than that obtained at $\phi_V = 0.43$. It is likely that

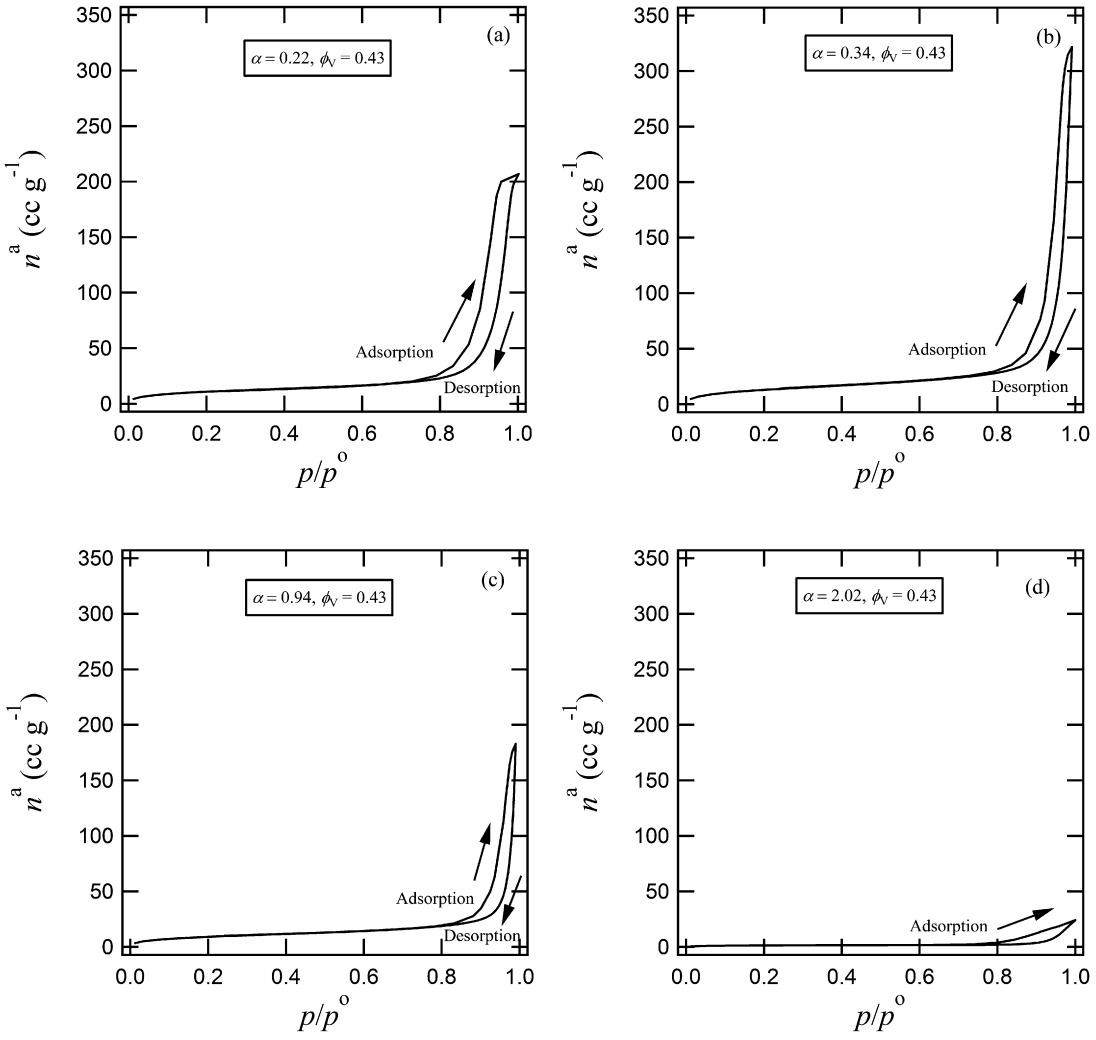

Fig. 2. Results of N_2 physisorption experiments. Plots of N_2 adsorbed as a function of p/p^o where p is the equilibrium pressure, and p^o is the saturation pressure at void fraction, $\phi_V = 0.43$ for normalized chain lengths of the sacrificial homopolymer, (a) $\alpha = 0.22$, (b) $\alpha = 0.34$, (c) $\alpha = 0.94$ and (d) $\alpha = 2.02$. Celgard® 2400 data are shown in Fig. S1.

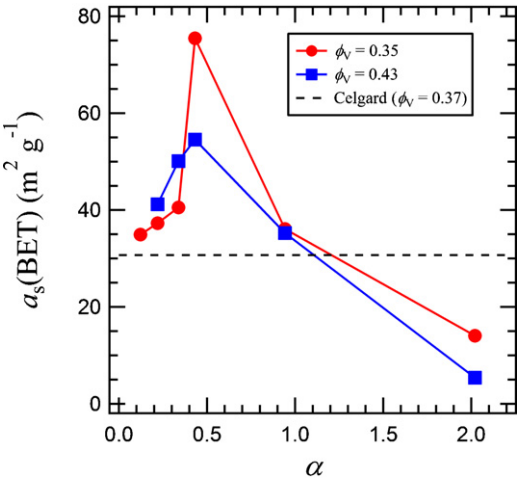

Fig. 3. Internal surface area measured by BET, a_s(BET) as a function of the normalized chain length of the sacrificial homopolymer, α, for select values of void fraction, ϕ_V, where the dashed line represents the a_s(BET) of Celgard® 2400.

the pore structure is well connected at $\phi_V = 0.43$ but poorly connected at $\phi_V = 0.16$. Increasing ϕ_V to 0.29 and 0.35 results in an increase in σ, as seen in Fig. 5b. There is, however, a concomitant increase in the error associated with the measurement of σ. The error bars decrease when ϕ_V is increased to 0.43. One explanation for the observed changes in the error bars is that it is difficult to obtain reproducible pore structures in the cross-over region between poorly connected ($\phi_V = 0.16$, Fig. 5b) and well-connected ($\phi_V = 0.43$, Fig. 5a) pores. The dashed lines in Fig. 5b represent average values of σ for each of the ϕ_V values. The conductivity data are summarized in Fig. 6, which shows the dependence of σ on ϕ_V and α. At $\phi_V = 0.16$, 0.29, and 0.35, we show the average value of σ. In this range, we find the expected trend of increasing conductivity with increasing ϕ_V. At $\alpha = 0.22$, this trend continues. Clearly, the $\alpha = 0.22$, $\phi_V = 0.43$ membrane exhibits the highest conductivity of the block copolymer separators obtained thus far. This conductivity is comparable to that of Celgard® 2400, which is also shown in Fig. 6. It is worth noting, however, that the Celgard membrane performance is more impressive because it has a lower void fraction than the optimized block copolymer membrane. This is, perhaps, not surprising, as the Celgard technology has been optimized for several years and is made using the dry process which leads to a reduction in tortuosity. In future work we will optimize

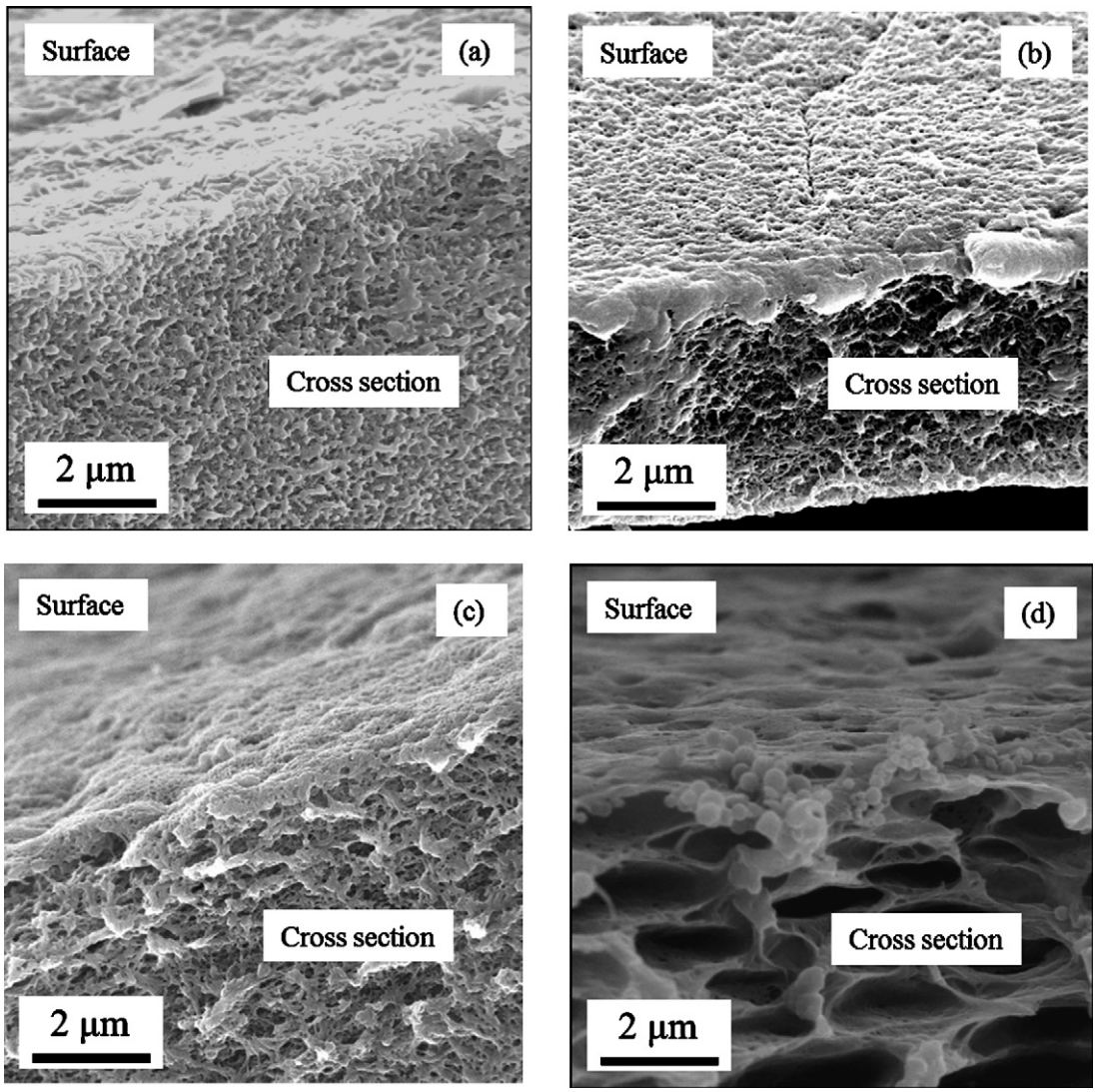

Fig. 4. Scanning electron micrographs of separators with void fraction, $\phi_V = 0.43$ at the normalized chain length of the sacrificial homopolymer, (a) $\alpha = 0.12$, (b) $\alpha = 0.22$, (c) $\alpha = 0.43$ and (d) $\alpha = 2.02$ obtained by cryofracturing washed out films. Celgard® 2400 data are shown in Fig. S2.

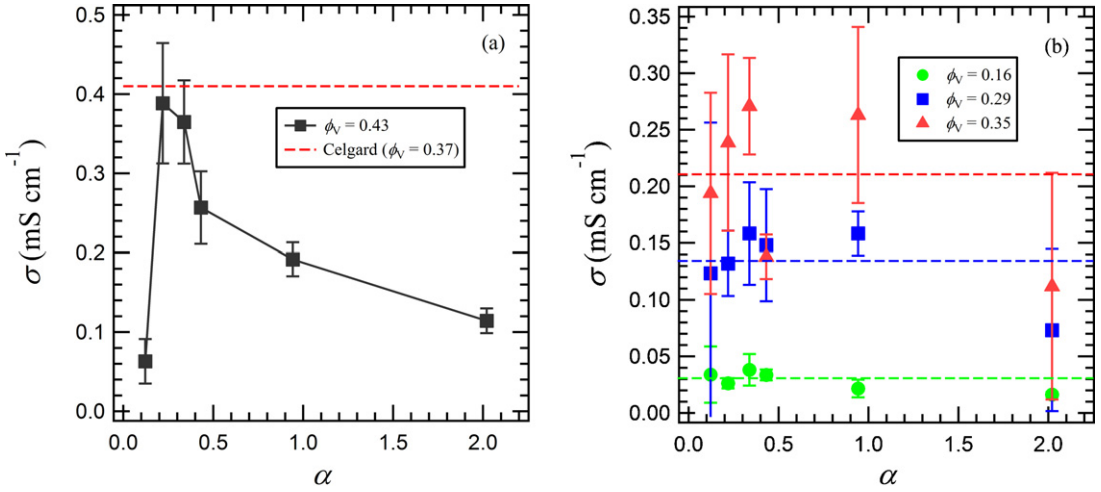

Fig. 5. Ionic conductivity, σ, of SES separators soaked in 1 M $LiPF_6$/EC/DEC as a function of the normalized chain length of the sacrificial homopolymer, α for (a) void fraction, $\phi_V = 0.43$, where the dashed line represents the conductivity of Celgard® 2400 in the same electrolyte, shown for comparison, and (b) ϕ_V of 0.16, 0.29, and 0.35, where the dashed lines represent the average α of the corresponding ϕ_V.

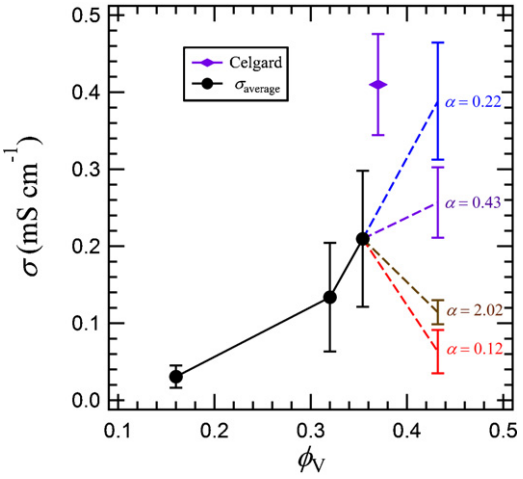

Fig. 6. Ionic conductivity, σ, of SES separators soaked in 1 M $LiPF_6$/EC/DEC as a function of void fraction, ϕ_V, where σ at ϕ_V of 0.16, 0.29, and 0.35 is the average value across all values of α. σ at $\phi_V = 0.43$ is plotted at $\alpha = 0.22$, 0.43, 2.02, and 0.12.

the block copolymer-based separators and examine the possibility of outperforming current separators.

3.3. SAXS

The SAXS profile of pure SES copolymer at 140 °C, shown in Fig. 7, exhibits a broad primary peak at $q = q^* = 0.14\,nm^{-1}$ and a shoulder at higher q values. The width of the primary peak indicates that the SES sample has relatively little long-range order. This may be a due to a combination of effects such as the complexity of the sample (an incompletely coupled triblock copolymer) and the processing steps used to create the sample. However, we expect the SES sample to contain hexagonally packed PS cylinders in a PE matrix, based on a polystyrene volume fraction of 0.23. The domain size of the morphology, $d = 2\pi/q^* = 45$ nm. The higher order shoulder is attributed to a combination of the expected higher order peaks of the hexagonal phase at $q = \sqrt{3}q^*$ and $2q^*$. In contrast, SAXS data from SES/PS mixtures generally did not contain scattering peaks that could be easily interpreted in terms of morphology, particularly at the high values of ϕ_V that are of practical interest. In Fig. 7, we show the scattering profiles of SES/PS blends with $\alpha = 0.22$ and $\phi_V = 0.43$ at 140 °C. The presence of a shoulder in the vicinity of $q = q^*$ suggests the presence of a characteristic length scale of about 45 nm. The absence of well-defined peaks indicates the lack of a simple periodic morphology. SAXS profiles obtained from the SES/PS blends with $\alpha = 0.22$ and $\phi_V = 0.43$ at 25 °C before and after washing, shown in Fig. 7, also contain shoulders in the vicinity of $q = q^*$. However, these data are affected by the semicrystalline nature of the PE block in the SES copolymer which can suppress the ordering of the block copolymer [22–29]. The length scale of the pores seen in the SEM data (Fig. 4b) are outside the q-window available in SAXS. The SAXS data provide weak support for the presence of microphase separation of PE and PS domains on the 45 nm length scale.

3.4. Discussion

The main observation of this study is that α, the normalized chain length of the sacrificial homopolymer, has a profound effect on membrane conductivity (Figs. 5 and 6). It is likely that this observation is a reflection of the morphology of the SES/PS film before the THF-washing step. However, based on very general arguments presented by Shull [44] and Leibler [45], one expects the morphology of blends of A-B-A triblock copolymers and A homopolymers to depend on α. If $\alpha \ll 1$, then the A homopolymer is compatible with

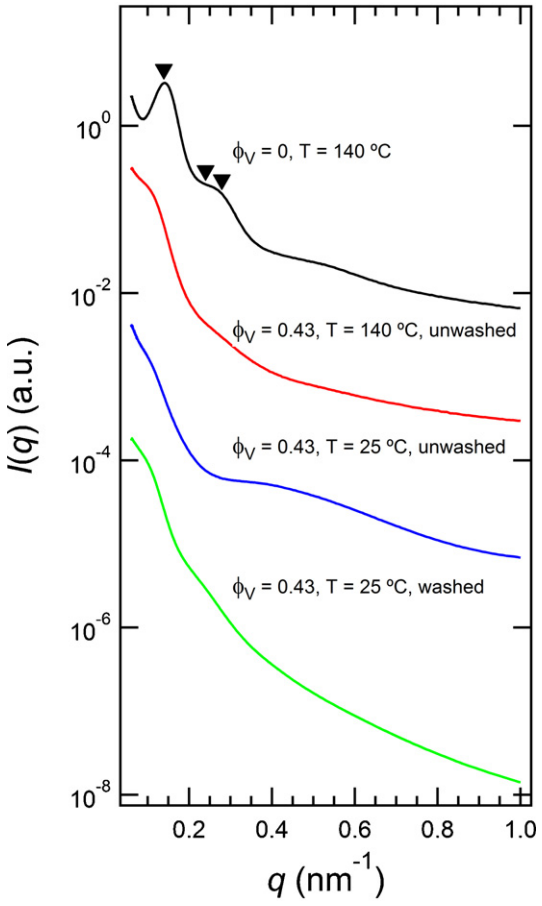

Fig. 7. SAXS profile of SES copolymer and SES/PS copolymer blends before and after washing with intensity (a.u.), I, as a function of scattering vector, q (nm^{-1}). ϕ_V is used to represent the volume fraction of PS homopolymer blended. The top profile represents the neat block copolymer. The annotations on the top profile represent the $q*$, $\sqrt{3}q^*$, and $2q*$ positions. The middle two profiles have homopolymer added, but the homopolymer has not been washed out. The bottom profile was taken after washing out homopolymer PS. The PS homopolymer for this blend is $\alpha = 0.22$.

both A and B blocks and will thus be distributed uniformly in both blocks. Dissolving out the homopolymer in such a film will result in extremely small pores on the length scale of the A homopolymer (which is a very short chain) located in both A and B microdomains. On the other hand, if $\alpha \gg 1$ then the homopolymer is expected to form separate macroscopic domains. Dissolving out the homopolymer in such a film will result in macroscopic pores. The localization of A homopolymer in the A microdomains of the block copolymer is only expected over an intermediate range of values of α. Dissolving out the homopolymer in such a film will result in nanoscale pores. This provides an explanation for the observed dependence of conductivity on α at $\phi_V = 0.43$, reported in Fig. 5a. At $\alpha = 0.12$, the homopolymer chain length is too small and it is distributed homogeneously in the PS-rich and PE-rich microphases. Thus, when the homopolymer is extracted from this sample, a membrane with very small voids that are unrelated to the block copolymer morphology are formed (Fig. 4a). In contrast, at $\alpha = 2.02$, the homopolymer chain length is too large and it macrophase-separates into micron-sized domains leading to the large pores seen in Fig. 4d. One might anticipate that the pores in Fig. 4d are more effective for transport than the small pores in Fig. 4a. The transport measurements shown in Figs. 5 and 6 indicate otherwise. The porous structures shown in both Fig. 4a and d are equally ineffective for transport. Nanoscale pores that are effective for transport are only seen at intermediates values of α, such as $\alpha = 0.22$ (Fig. 4b) and $\alpha = 0.43$ (Fig. 4c). The effect

of morphology on transport is dramatic. At $\phi_V = 0.43$, the ionic conductivity of the sample with $\alpha = 0.22$ is 6 times greater that of the sample with $\alpha = 0.12$. The a_s(BET) trends shown in Fig. 3 are qualitatively similar to the conductivity trends reported in Fig. 5a. The shapes of the curves in Figs. 3 and 5a are different, the former is peaked at $\alpha = 0.43$, while the latter is peaked at $\alpha = 0.22$. We do not have an explanation for these differences. It is clear that a complete understanding of the present system requires a study of the morphology of the polymer films before washing out the homopolymer. We will address this issue in future publications.

4. Conclusions

Nanoporous battery separators were made by casting films of block copolymer/homopolymer blends and selectively removing the homopolymer. The volume occupied by homopolymer chains in cast films are thus converted into pores. This approach enabled systematic variation of the pore structure at fixed void fraction by changing the normalized chain length of the sacrificial homopolymer, α. The efficacy of the separators thus obtained was determined by measurement of the ionic conductivity of separators soaked in a standard liquid electrolyte. In highly porous separators with a fixed pore volume fraction of 0.43, conductivity was peaked at $\alpha = 0.22$. Nitrogen adsorption and SEM were used to determine the underpinnings of this observation. At low values of α, conductivity is low because very small, poorly connected pores are formed. At high values of α, conductivity is low because very large pores are formed.

Acknowledgements

This work was conducted within the Batteries for Advanced Transportation Technologies (BATT) Program, supported by the U.S. Department of Energy Vehicle Technologies Program under Contract No. DE-AC02-05CH11231. The Advanced Light Source is supported by the Director, Office of Science, Office of Basic Energy Sciences, of the U.S. Department of Energy under Contract No. DE-AC02-05CH11231. The authors thank Greg Stone and Alexander Teran for their help in AC impedance spectroscopy measurements. The authors also thank Xiangyun Song for assistance in nitrogen adsorption experiments.

Appendix A. Supplementary data

Supplementary data associated with this article can be found, in the online version, at doi:10.1016/j.memsci.2011.12.037.

References

[1] L.C. Gaines, R. Cuenca, in: Department of Energy (Ed.), Costs of Lithium-ion Batteries for Vehicles, 2000, Argonne, IL.
[2] D. Ihm, J. Noh, J. Kim, Effect of polymer blending and drawing conditions on properties of polyethylene separator prepared for Li-ion secondary battery, Journal of Power Sources 109 (2002) 388–393.
[3] M.J. Weighall, Recent advances in polyethylene separator technology, Journal of Power Sources 34 (1991) 257–268.
[4] S.S. Zhang, A review on the separators of liquid electrolyte Li-ion batteries, Journal of Power Sources 164 (2007) 351–364.
[5] N.P. Balsara, Multicomponent polyolefin blends with ordered and disordered microstructures, Current Opinion in Solid State and Materials Science 3 (1998) 589–595.
[6] S. Datta, D.J. Lohse, Graft Copolymer Compatibilizers for blends of isotactic polypropylene and ethene propene copolymers. 2. Functional polymers approach, Macromolecules 26 (1993) 2064–2076.
[7] H.S. Jeon, J.H. Lee, N.P. Balsara, Predictions of the thermodynamic properties of multicomponent polyolefin blends from measurements on two-component systems, Macromolecules 31 (1998) 3328–3339.
[8] A.A. Lefebvre, J.H. Lee, H.S. Jeon, N.P. Balsara, B. Hammouda, Initial stages of nucleation in phase separating polymer blends, Journal of Chemical Physics 111 (1999) 6082–6099.
[9] D.J. Lohse, The melt compatibility of blends of polypropylene and ethylene–propylene copolymers, Polymer Engineering and Science 26 (1986) 1500–1509.
[10] P.G. De Gennes, Reptation of a polymer chain in presence of fixed obstacles, Journal of Chemical Physics 55 (1971) 572–579.
[11] J.D. Ferry, Viscoelastic Properties of Polymers, 3rd ed., John Wiley & Sons, 1980.
[12] W.W. Graessley, Polymeric Liquids & Networks: Dynamics and Rheology, Taylor & Francis Group, LLC, London, 2008.
[13] P.I. Flory, Thermodynamics of high polymer solutions, Journal of Chemical Physics 10 (1942) 51–61.
[14] M.L. Huggins, Some properties of solutions of long-chain compounds, Journal of Physical Chemistry 46 (1942) 151–158.
[15] N.A. Lynd, M.A. Hillmyer, Influence of polydispersity on the self-assembly of diblock copolymers, Macromolecules 38 (2005) 8803–8810.
[16] L.M. Pitet, M.A. Amendt, M.A. Hillmyer, Nanoporous linear polyethylene from a block polymer precursor, Journal of the American Chemical Society 132 (2010) 8230–8231.
[17] A.V. Ruzette, S. Tence-Girault, L. Leibler, F. Chauvin, D. Bertin, O. Guerret, P. Gerard, Molecular disorder and mesoscopic order in polydisperse acrylic block copolymers prepared by controlled radical polymerization, Macromolecules 39 (2006) 5804–5814.
[18] J.M. Widin, A.K. Schmitt, K. Im, A.L. Schmitt, M.K. Mahanthappa, Polydispersity-induced stabilization of a disordered bicontinuous morphology in ABA triblock copolymers, Macromolecules 43 (2010) 7913–7915.
[19] F.S. Bates, G.H. Fredrickson, Block copolymer thermodynamics – theory and experiment, Annual Review of Physical Chemistry 41 (1990) 525–557.
[20] L. Leibler, Theory of microphase separation in block copolymers, Macromolecules 13 (1980) 1602–1617.
[21] M.W. Matsen, F.S. Bates, Unifying weak- and strong-segregation block copolymer theories, Macromolecules 29 (1996) 1091–1098.
[22] Y.L. Loo, R.A. Register, A.J. Ryan, Polymer crystallization in 25-nm spheres, Physical Review Letters 84 (2000) 4120–4123.
[23] Y.L. Loo, R.A. Register, A.J. Ryan, Modes of crystallization in block copolymer microdomains: breakout, templated, and confined, Macromolecules 35 (2002) 2365–2374.
[24] Y.L. Loo, R.A. Register, A.J. Ryan, G.T. Dee, Polymer crystallization confined in one, two, or three dimensions, Macromolecules 34 (2001) 8968–8977.
[25] D.J. Quiram, R.A. Register, G.R. Marchand, Crystallization of asymmetric diblock copolymers from microphase-separated melts, Macromolecules 30 (1997) 4551–4558.
[26] I.W. Hamley, J.P.A. Fairclough, F.S. Bates, A.J. Ryan, Crystallization thermodynamics and kinetics in semicrystalline diblock copolymers, Polymer 39 (1998) 1429–1437.
[27] I.W. Hamley, J.P.A. Fairclough, N.J. Terrill, A.J. Ryan, P.M. Lipic, F.S. Bates, E. Towns-Andrews, Crystallization in oriented semicrystalline diblock copolymers, Macromolecules 29 (1996) 8835–8843.
[28] A.J. Ryan, I.W. Hamley, W. Bras, F.S. Bates, Structure development in semicrystalline diblock copolymers crystallizing from the ordered melt, Macromolecules 28 (1995) 3860–3868.
[29] H. Schmalz, A. Knoll, A.J. Muller, V. Abetz, Synthesis and characterization of ABC triblock copolymers with two different crystalline end blocks: influence of confinement on crystallization behavior and morphology, Macromolecules 35 (2002) 10004–10013.
[30] C. Caze, S.H. Pak, Inherent polarity of polystyrene upon miscibility in incompatible blends with low-density polyethylene, Journal of Materials Science Letters 16 (1997) 53–55.
[31] S. Wu, Surface and interfacial tensions of polymer melts. 2. Poly(methyl methacrylate), poly(normal-butyl methacrylate) and Polystyrene, Journal of Physical Chemistry 74 (1970) 632–638.
[32] W.A. Phillip, J. Rzayev, M.A. Hillmyer, E.L. Cussler, Gas and water liquid transport through nanoporous block copolymer membranes, Journal of Membrane Science 286 (2006) 144–152.
[33] H. Uehara, M. Kakiage, M. Sekiya, D. Sakuma, T. Yamonobe, N. Takano, A. Barraud, E. Meurville, P. Ryser, Size-selective diffusion in nanoporous but flexible membranes for glucose sensors, ACS Nano 3 (2009) 924–932.
[34] S.Y. Yang, I. Ryu, H.Y. Kim, J.K. Kim, S.K. Jang, T.P. Russell, Nanoporous membranes with ultrahigh selectivity and flux for the filtration of viruses, Advanced Materials 18 (2006) 709–712.
[35] S.Y. Yang, J.A. Yang, E.S. Kim, G. Jeon, E.J. Oh, K.Y. Choi, S.K. Hahn, J.K. Kim, Single-file diffusion of protein drugs through cylindrical nanochannels, ACS Nano 4 (2010) 3817–3822.
[36] N. Zhou, F.S. Bates, T.P. Lodge, Mesoporous membrane templated by a polymeric bicontinuous microemulsion, Nano Letters 6 (2006) 2354–2357.
[37] M. Morton, L.J. Fetters, Anionic polymerization of vinyl monomers, Rubber Chemistry and Technology 48 (1975) 359.
[38] Y.C. Lin, R.C.C. Tsiang, Using heavy ethers as structure modifiers in the synthesis of SBS block copolymers in cyclohexane, Journal of Applied Polymer Science 64 (1997) 2543–2560.
[39] S.F. Hahn, An improved method for the diimide hydrogenation of butadiene and isoprene containing polymers, Journal of Polymer Science Part A: Polymer Chemistry 30 (1992) 397–408.
[40] J.E. Mark, H.B. Eitouni, N.P. Balsara, Thermodynamics of polymer blends, in: Physical Properties of Polymers Handbook, Springer, New York, 2007, pp. 339–356.
[41] J. Brandrup, E.H. Immergut, Polymer Handbook, 3rd ed., John Wiley & Sons, New York, 1989.

[42] S. Brunauer, P.H. Emmett, E. Teller, Adsorption of gases in multimolecular layers, Journal of the American Chemical Society 60 (1938) 309–319.
[43] K.S.W. Sing, D.H. Everett, R.A.W. Haul, L. Moscou, R.A. Pierotti, J. Rouquerol, T. Siemieniewska, Reporting physisorption data for gas solid systems with special reference to the determination of surface-area and porosity (recommendations 1984), Pure and Applied Chemistry 57 (1985) 603–619.
[44] K.R. Shull, Theory of end-adsorbed polymer brushes in polymeric matrices, Journal of Chemical Physics 94 (1991) 5723–5738.
[45] L. Leibler, Emulsifying effects of block copolymers in incompatible polymer blends, Makromolekulare Chemie-Macromolecular Symposia 16 (1988) 1–17.